IEEE Access
Multidisciplinary | Rapid Review | Open Access Journal

Received December 21, 2018, accepted January 14, 2019, date of publication January 24, 2019, date of current version February 12, 2019.

Digital Object Identifier 10.1109/ACCESS.2019.2894812

Wideband Low-Profile Printed Dipole Antenna Incorporated With Folded Strips and Corner-Cut Parasitic Patches Above the Ground Plane

KAM EUCHARIST KEDZE[1], HEESU WANG[1], SON XUAT TA[2], AND IKMO PARK[1]

[1]Department of Electrical and Computer Engineering, Ajou University, Suwon 16499, South Korea
[2]School of Electronics and Communications, Hanoi University of Science and Technology, Hanoi 100000, Vietnam

Corresponding author: Ikmo Park (ipark@ajou.ac.kr)

This work was supported in part by the National Research Foundation of Korea (NRF) Grant funded by the Korea Government (MSIT) under Grant 2018R1D1A1A02086071, and in part by the Institute for Information and Communications Technology Promotion (IITP) Grant through the Korea Government (MSIP), University ICT Basic Research Lab, under Grant 2017-0-00959.

ABSTRACT In this paper, the design of a wideband high-gain low-profile linearly polarized antenna is presented. The design objectives were achieved by encircling a folded strip around a planar radiating element on the top substrate with corner-cut parasitic patches on the bottom substrate placed above the ground plane. A half-wavelength printed dipole utilized as a radiating element was employed to generate linearly polarized radiation. The contributions of the folded strips and parasitic patches are significant factors in enhancing the bandwidth by producing extra resonance and phase compensation. The experiments and full-wave electromagnetic simulations have provided a platform for the analysis, validation, and verification of the antenna design. The antenna structure has the overall dimensions of 120 mm × 120 mm × 16.3 mm ($0.69\lambda_o \times 0.69\lambda_o \times 0.094\lambda_o$ at 1.74 GHz), and it demonstrated satisfactory measured performance characteristics with a −10-dB impedance bandwidth of 1.39–2.09 GHz (40.22%), a broadside gain of 6.1–8.2 dBi, and a radiation efficiency >88% within the impedance bandwidth.

INDEX TERMS Folded strip, low-profile antenna, parasitic patch, planar antenna, printed dipole, wideband.

I. INTRODUCTION

A horizontally positioned dipole above a perfect electric conducting ground plane at a small fraction of the operating wavelength has gained significant interest for low-profile antenna designs. It is well known that a dipole antenna is horizontally positioned at a quarter wavelength distance above a ground plane or perfect electric conductor (PEC) to accomplish high broadside gain through in-phase reflection [1]. However, when a dipole is placed horizontally over a PEC ground plane, an image current exists that is out of phase to that of the radiating dipole. As the distance between the dipole and the PEC ground plane approaches zero, the total radiated far electric field diminishes in all directions because the direct and image currents tend to cancel out each other [2]. Furthermore, with the close spacing of two current elements (the dipole's source and image current) that are nearly 180° out of phase, there is a substantial increase in the reactive energy surrounding the dipole, resulting in a substantial decrease in the dipole's operating bandwidth. Ultimately, a narrow bandwidth is the main factor that limits performance when a dipole element is closely spaced to a highly conducting ground plane [3].

To overcome this problem of antenna performance degradation, several approaches have been developed. One approach applies the principle behind artificial surfaces such as electromagnetic bandgaps (EBGs) and artificial magnetic conductors (AMCs) [4]–[7]. The reflection phase of an EBG surface can, in general, vary from −180° to +180°, which makes the EBG more versatile and unique [8]. These surfaces can be employed to manipulate or control the phases of the reflected fields for dipoles in proximity to the ground plane [9]–[18]. An impedance bandwidth of 16% with a peak gain of 6.7 dBi was recorded for a dipole at a height of $0.07\lambda_o$ above an EBG ground plane [16]. Another result achieved a bandwidth of 0.07% and a peak gain of 5.2 dBi at a height of $0.05\lambda_o$ when the dipole was placed upon a split ring resonator-based ground plane surface [2].

Other approaches have produced considerable results for a dipole horizontally placed above the ground plane. These approaches improve the impedance matching of the antenna

by reconfiguring the antenna structure to alter its radiation resistance and thereby improve the radiation properties [19]. For instance, a VSWR <3 bandwidth of 2.2% was achieved with a thin wire dipole and a folded arm radiator above the ground plane [20]. A notable achievement was lately recognized whereby through the phase compensation mechanism with a parasitic strip, an impedance bandwidth of 0.6%, a gain of 7.8 dBi, and an efficiency of 74% were attained for a dipole horizontally placed in proximity above the ground plane at a low profile [21]. Nevertheless, these antenna structures can be generalized as having limited impedance bandwidth capabilities. Most recently, another significant performance improvement was attained at a low profile by inserting a circular parasitic patch, which was divided into four equal segments by two orthogonal slots, between a planar dipole element and the ground plane [22]. The parasitic patches were inserted to achieve profile miniaturization and bandwidth enhancement. The antenna was characterized with an $|S_{11}| < -10$ dB bandwidth of 1.465–1.740 GHz (17.2%), a broadside gain of 8.5–8.8 dBi, and a radiation efficiency >96% at a height of $0.087\lambda_o$.

Ultra wideband (UWB) monopoles have provided broad bandwidths. Nonetheless, UWB monopoles fall short in some applications requiring low-profile, high-gain, and broadside radiation patterns [23]–[26]. Magneto-electric dipoles have certain advantages, such as a wide bandwidth, high directivity, low cross-polarization, and low back lobe radiation. Yet, noticeable shortcomings of the magneto-electric dipole are its high-profile structure and large ground plane size, which might render it inappropriate for applications where a low profile and small size structure are required [27]–[36]. Recently, a bandwidth-enhanced cavity-backed magneto-electric dipole achieved a broad bandwidth of 88% for a $S_{11} \leq -15$ dB. However, the antenna had a large ground plane coupled with a high profile of $0.36\lambda_o$ [32]. A compact magneto-electric dipole for the LTE femtocell base station was proposed to achieve a bandwidth of 65.7% for a $S_{11} \leq -10$ dB, but its profile of $0.20\lambda_o$ is an impediment in extremely low-profile applications [34]. On the other hand, a low profile magneto-electric dipole with a ground plane size of $1\lambda_o \times 1\lambda_o$ achieved a bandwidth of 28.2% for a VSWR$\leq$2 with a profile of $0.097\lambda_o$; nevertheless, its limited bandwidth may inadequate for several wideband applications [35].

This paper expands on [37] and presents details of a wideband low-profile antenna with a folded strip encircling a planar radiating element and corner-cut parasitic patches above the ground plane. The patches are used to improve the impedance matching and control the phase interaction between the dipole and the ground plane that are in proximity, while the folded strips above the parasitic patches are significant for bandwidth improvement. The fabricated antenna achieves a measured −10 dB impedance bandwidth of 1.39–2.09 GHz (40.22% with respect to the center frequency of 1.74 GHz) and a peak gain of 8.2 dBi with overall dimensions of 120 mm × 120 mm × 16.3 mm ($0.69\lambda_o \times 0.69\lambda_o \times 0.094\lambda_o$ at 1.74 GHz).

The remainder of this paper is structured as follows. In Section II, a guideline of the antenna design procedure is presented, which is followed by explanations of the antenna operational modes, radiation mechanisms, and an illustration of the antenna performance characteristics. Section III describes the response of the antenna when there is a variation in each of its parameters. The experimental setup and measurement results are discussed in Section IV, and in Section V conclusions are drawn.

II. ANTENNA GEOMETRY AND PERFORMANCE

The geometry of the proposed antenna is shown in Fig. 1. The antenna configuration is composed of a printed dipole element, folded strips, parasitic patches, a ground plane, and

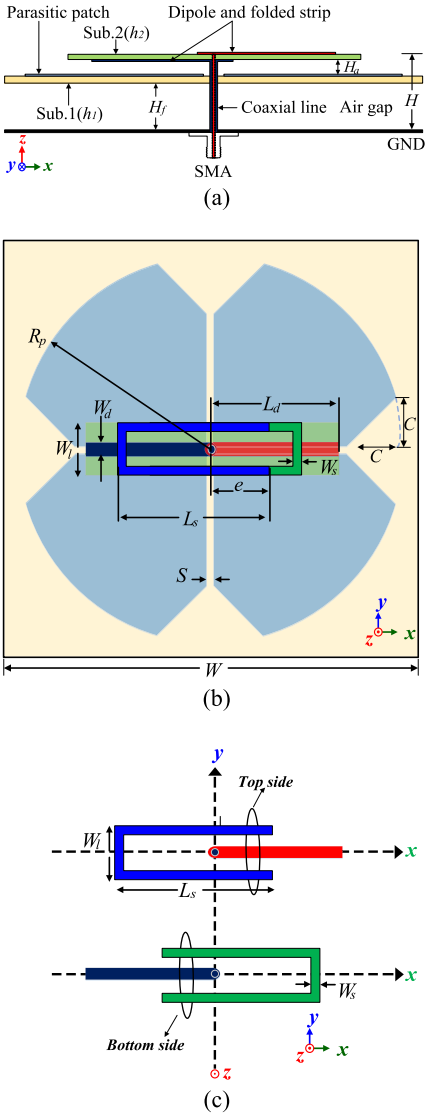

FIGURE 1. Geometry of the antenna: (a) side view, (b) top view, and (c) extended view of folded strip and dipole.

a coaxial feed. The dipoles and folded strips are printed on the top and bottom sides of substrate 2, and the printed parasitic patches are printed on the top side of substrate 1. Both substrates are made of Rogers RO4003 material and are identical with $\varepsilon_r = 3.38$, $tan\delta = 0.0027$, and $h_1 = h_2 = 0.8128$ mm, and are horizontally placed in proximity above the ground plane. The parasitic patches are formed by dividing a circular patch with two perpendicular slots into four identical patches. Two isosceles right triangle subtractions were made at the edges of each of the four patches. The folded strips are designed to encircle the dipoles in a loop configuration with one side completely open. The folded strips are placed on both sides of substrate 2, making sure the strips overlap considerably. The single center-fed printed dipole is excited through a coaxial line with a characteristic impedance of 50 Ω. The outer conductor of the coaxial line is connected to the bottom arm of the dipole. The inner conductor of the coaxial line extends through substrate 2 and connects to the top half of the dipole [38]. The antenna attained a low profile and a broadband characteristic at a center frequency of approximately 1.76 GHz as characterized by ANSYS HFSS software. The antenna's optimum design parameters are as follows: $W = 120$ mm, $H_f = 12.7$ mm, $C = 12$mm, $H_a = 2$ mm, $R_p = 60$ mm, $S = 5.2$ mm, $L_d = 35$ mm, $W_d = 4.3$ mm, $h_1 = h_2 = 0.8128$ mm, $H = 16.3$ mm, $W_s = 0.5$ mm, $W_l = 11.2$ mm, $L_s = 36.1$ mm, $e = 4.1$ mm.

The proposed design attains a low profile with an overall antenna height of $0.094\lambda_o$, which is substantially less than the optimum spacing (0.25λ) for a dipole above the ground plane. This is feasible through the insertion of the parasitic patches that minimize the effects of the reflected fields and image currents from the ground plane while enabling the dipole and folded strips to radiate efficiently. By reducing the spacing (antenna height) between the dipole element and the ground plane, the radiated fields and out-of-phase reflected fields converge destructively, and consequently degrade antenna bandwidth performance. Accordingly, the parasitic patches on the lower substrate are crucial to compensate for the out-of-phase reflected fields and diminish the effects of destructive interference [21].

The parasitic patches, while performing phase compensation, are also active in generating resonance that improves the impedance bandwidth. The contribution of the folded strips is noticeable in bandwidth improvement. The involvement of the folded strip generates additional resonance at high frequencies that widen the antenna impedance bandwidth. The folded strips are encircled around the dipole to provide a wide area for electromagnetic interactions between the dipole and the folded strips and to increase the coupling between both elements. Both folded strips are overlapped together to act as a half-wavelength antenna, like arms of a dipole. The overlapping is a prerequisite for both folded strips to be sufficiently excited and hence resonate at high frequencies.

To thoroughly understand the role of the corner-cut parasitic patches and folded strips in bandwidth enhancement, detailed structural comparison of the antenna in four different

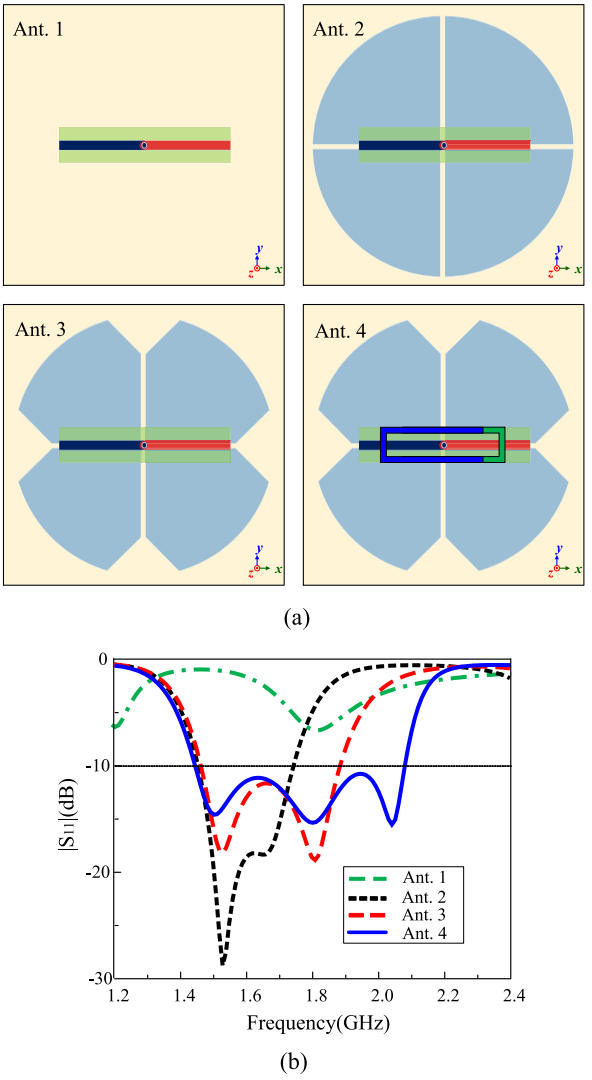

FIGURE 2. **(a) Different configurations of the dipole antenna and (b) $|S_{11}|$ values of the dipole antenna for the different antenna configurations.**

configurations was performed, as shown in Fig. 2(a). Ant. 1 is a single dipole antenna without parasitic patches. Ant. 2 is a single dipole antenna with parasitic patches as presented in [22]. Ant. 3 is a single dipole with the corner-cut parasitic patches. Ant. 4 is the proposed antenna design consisting of a dipole with folded strips and corner-cut parasitic patches. All four antennas have the same configurations in height ($0.094\lambda_o$), overall size, substrate thickness, and type. As shown in Fig. 2(b), Ant. 1 produces single resonance from the dipole element with very poor impedance matching. Ant. 2 generates two resonances in its reflection coefficient profiles: one from the parasitic patches and the other from the dipole. The resonance from the patches is clearly noticeable, whereas that of the dipole is directly adjacent and merges to that of the parasitic patches because of under-coupling. Ant. 3 generates two noticeable resonances in its reflection coefficient profile. The first resonance is patch resonance whereas the corner-cut parasitic patches enable the dipole and

slot to be effectively coupled together, which consequently improves the bandwidth. Hence, the corner-cut parasitic patches widen the bandwidth of the antenna. Ant. 4 produces three distinguishable resonances. The first resonance occurs at 1.5 GHz and is generated by the parasitic patches. The dipole produces the second resonance at 1.8 GHz, and the third resonance at 2.02 GHz is a product of the folded strip. The three resonances mutually interact to produce a broad impedance bandwidth at a low profile. As shown in Fig. 2(b), the proposed design with an overall size of 120 mm × 120 mm × 16.3 mm yielded a simulated $|S_{11}| < -10$ dB impedance bandwidth of 1.44–2.08 GHz (36.36%) with three minimum points at 1.5, 1.8, and 2.02 GHz. Consequently, the antenna achieves profile miniaturization with significant bandwidth improvements compared to other designs of the dipole in proximity to the ground plane.

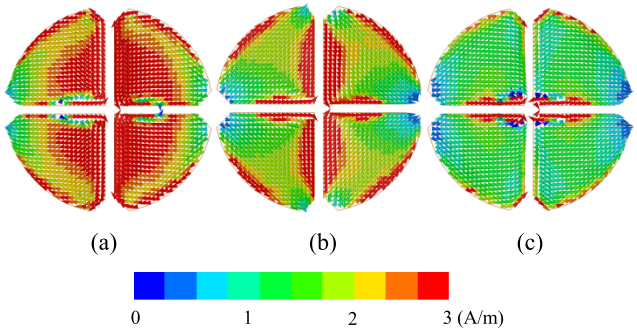

FIGURE 3. Surface current distributions on the parasitic patches: (a) 1.5 GHz, (b) 1.8 GHz, and (c) 2.02 GHz.

In order to comprehend the mechanism behind the three resonances, the current distribution on the parasitic patches, dipole, and folded strips are shown in Figs. 3 and 4. With the dipole and folded strips at proximity with the ground plane, there is an increase in reactive energy in the near field that results in an increased mutual coupling. The parasitic patches minimize the effects of mutual coupling from the ground plane and create an environment for the effective electromagnetic coupling between dipole and folded strips. Fig. 3 shows the current distribution of the parasitic patches at different frequency points. The intensity of the current on the patches at 1.5 GHz is higher than that of the other two resonant points. At 1.8 GHz and 2.02 GHz, the current intensity drops rapidly, particularly at 2.02 GHz, confirming the patches to be resonating at the low frequency of 1.5 GHz.

The surface current distributions of the dipole and folded strip at three frequency points are shown in Fig. 4. At 1.5 GHz, neither the dipole nor the folded strips exhibit strong currents, indicating that the parasitic patches alone resonate. A close observation at 1.8 GHz shows the dipole with a large proportion of strong current as compared to the patches and folded strips. The assembled currents on the dipole provide evidence of the dipole responsible for the intermediate frequency resonance at 1.8 GHz. Furthermore, at 2.02 GHz, it is clear from the current distribution that the folded strips

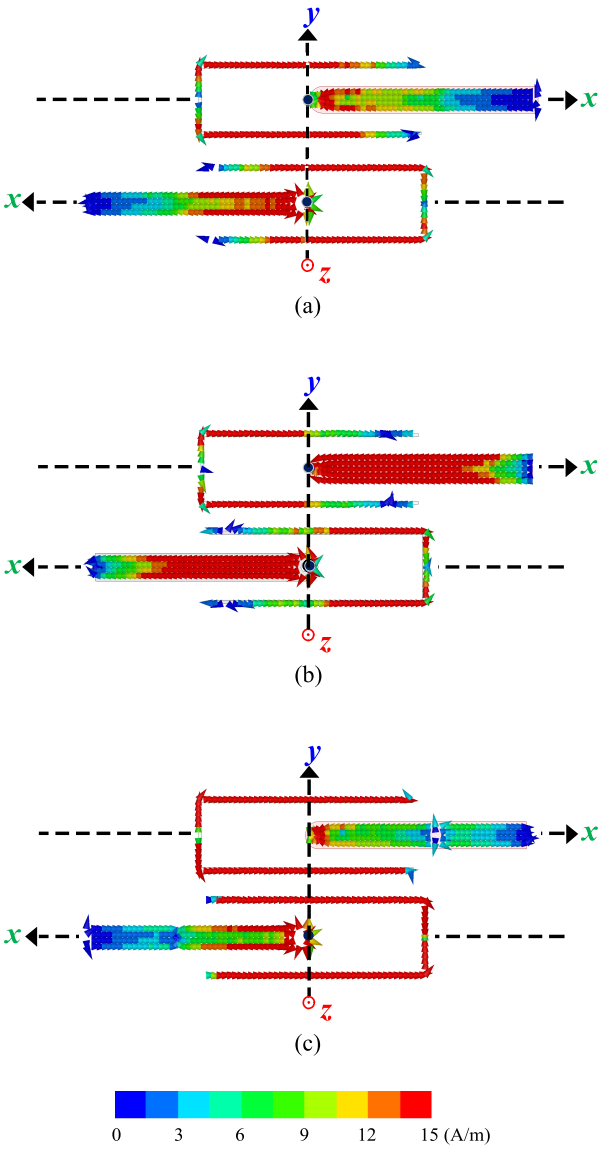

FIGURE 4. Surface current distributions on the dipole and folded strips: (a) 1.5 GHz, (b) 1.8 GHz, and (c) 2.02 GHz.

are responsible for this resonance. Heavy currents assemble on the folded strips exciting it to resonate at 2.02 GHz. At this resonant point of 2.02 GHz, neither the dipole nor the patches are excited. The currents are less intense, and they do not contribute to the high-frequency resonance. By observation, the scales in Figs. 3 and 4 are different because the current densities on the dipole and folded strips are much higher than on those of the patches. The reason being that the patches have a large surface area compared to the dipole and the folded strips.

III. PARAMETRIC STUDY

To achieve the antenna's optimum performance and to illustrate the effects of each parameter on the antenna characteristics, parametric investigations were performed on the

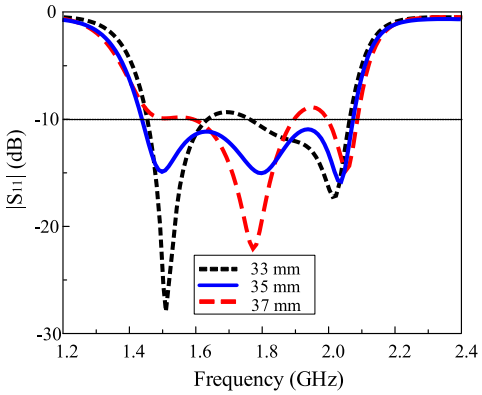

FIGURE 5. $|S_{11}|$ values of the dipole antenna for different dipole lengths (L_d).

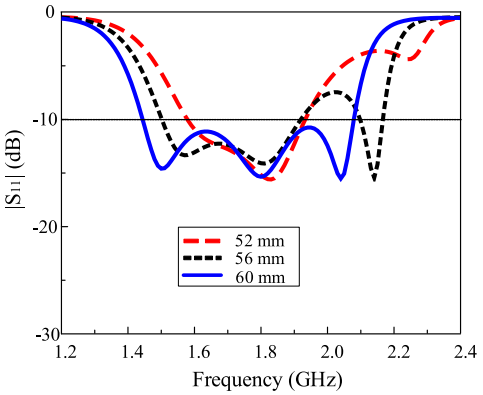

FIGURE 7. $|S_{11}|$ values of the dipole antenna for different sizes of parasitic patches (R_p).

antenna's design parameters. The antenna's responses were recorded after varying one parameter at a time from the optimized results.

The principal design parameters of the dipole are its length and width. As shown in Fig. 5, the effect of the dipole length can be observed by carefully examining the movement of the intermediate resonance as the dipole length changes. As the dipole length decreases, the intermediate resonance shifts to the right in the antenna reflection coefficient curve, because the resonant length changes and produces corresponding movements of the intermediate frequency resonance. This confirms that the dipole is responsible for the intermediate frequency resonance.

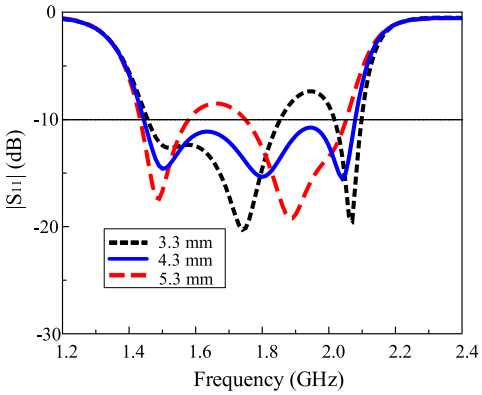

FIGURE 6. $|S_{11}|$ values of the dipole antenna for different dipole widths (W_d).

Fig. 6 shows the effects of dipole width on the antenna's performance. This parameter controls coupling between the dipole and the folded strips. For small dipole widths, coupling decreases, and for large dipole widths, coupling increases. The effect is significant at high frequencies where the dipole and folded strips resonate. At an optimum width of 4.3 mm, both elements are critically coupled, and their resonances interact to provide broad bandwidth at the high antenna frequencies.

Fig. 7 shows the reflection coefficient values of the antenna for different sizes of the parasitic patch. The patch size directly influences the low- and high-frequency resonances of the antenna. A change in the patch size moves the low-frequency resonance connoting that the patch is responsible for this resonance. As the patch size decreases, the first resonance moves to the right towards high frequencies while for large patch size it shifts towards low frequencies. In addition, the high-frequency resonance is affected by changes in patch size. As patch size reduces or for small patch size, the coupling between the folded strips and the parasitic patches significantly deteriorates and consequently causes the third or high frequency resonance to diminish and eventually disappears.

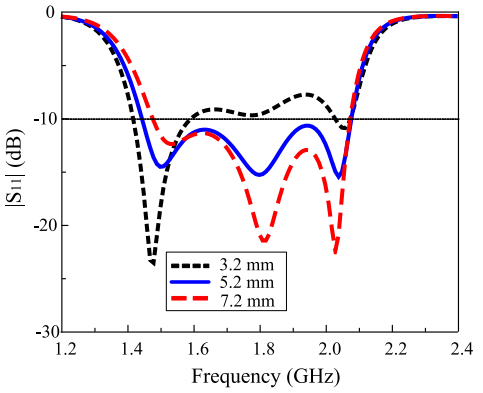

FIGURE 8. $|S_{11}|$ values of the dipole antenna for different parasitic patch separation values (S).

The separation between the patches (S) acts as a slot within the antenna. This S, also known as slot size (Fig. 1(b)), has an effect similar to that of the dipole width. Because the slot works in conjunction with the dipole, it therefore influences the effectiveness of the coupling between the dipole and the folded strips. As shown in Fig. 8, for small patch separation, the dipole and folded strips are strongly coupled, and for large

patch separation, the coupling is reduced. The slot size has an important role in the impedance matching of the antenna.

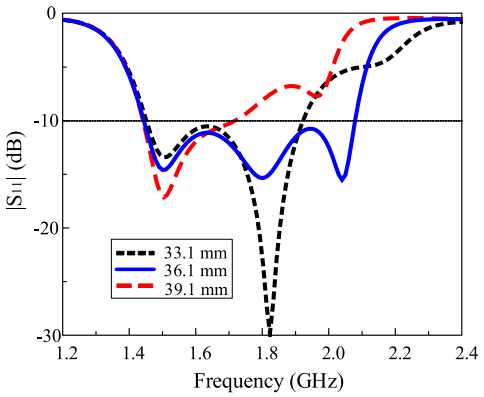

FIGURE 9. $|S_{11}|$ values of the dipole antenna for different folded strip lengths (L_s).

The folded strips have two design parameters: folded strip length (L_s) and width of the folded strips (W_l). From Fig. 9, more evidence is provided to validate the folded strip for the high-frequency resonance. An increase in folded strip length affects only the third resonance because the patch size and length of the dipole stay the same. Fig. 10 shows the effect of width of the folded strips on the coupling. This parameter influences the interaction between the dipole and folded strips. Accordingly, changes in this parameter is significant in controlling coupling. Consequently, their effects are important to the antenna impedance matching.

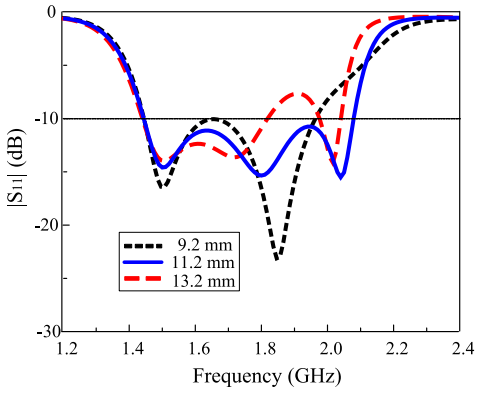

FIGURE 10. $|S_{11}|$ values of the dipole antenna for different folded strip widths (W_l).

Another significant parameter with a tremendous influence on the third resonance is the length of overlap ($2e$) between the folded strips. Both folded strips overlap considerably together to act as arms of a dipole and to radiate at a half wavelength. Therefore, the proportion of overlapping of both folded strips becomes a significant parameter to ensure that both strips are efficiently coupled together as a dipole. As shown in Fig. 11, the overlapping lengths increase as e increases. When the lengths of both folded strips

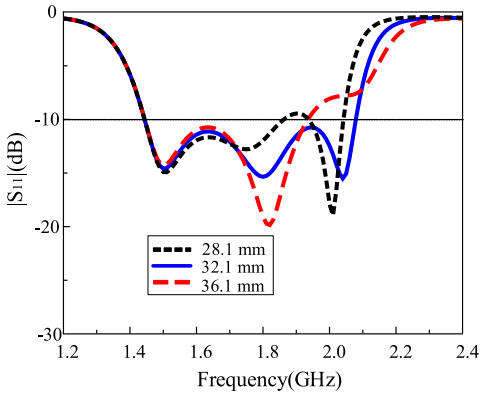

FIGURE 11. $|S_{11}|$ values of the dipole antenna for different folded strip overlap lengths (e).

completely overlap together ($2e = L_s$), both strips become over-coupled, and the high-frequency resonance diminishes. When e decreases, the coupling decreases and approaches critical coupling at a proper overlap length. At this point, both folded strips effectively resonate at high frequencies.

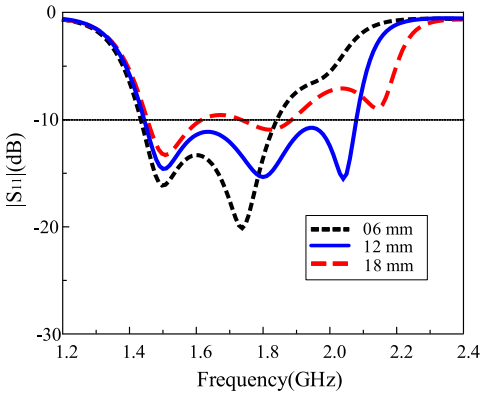

FIGURE 12. $|S_{11}|$ values of the dipole antenna for different sizes of corner cut (C).

The corner cut in the parasitic patch is crucial in increasing coupling and widening the antenna impedance bandwidth. Fig. 12 illustrates the significant role the corner cut plays in improving the antenna's impedance bandwidth. Bandwidth increases with increments in the corner cut (C). The corner cut effectively couples the dipole to the underside slot and to the folded strips at the same time. This allows both elements to be critically coupled and resonate efficiently. The ground plane size W has significant consequences on antenna performance. The size of the ground plane affects both the gain and front-to-back ratio, but has minimal effects on the impedance bandwidth. With a larger ground plane, the antenna generates almost the same impedance bandwidth with a more improved gain and front-to-back ratio.

IV. EXPERIMENTAL RESULTS

A fabricated sample of the proposed antenna is shown in Fig. 13. An Agilent N5230A network analyzer and

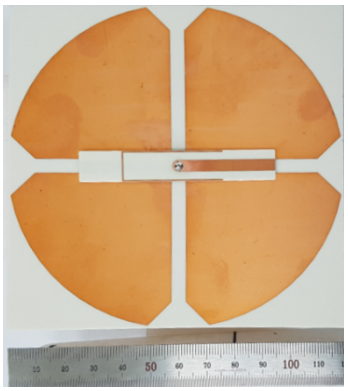

(a)

(b)

FIGURE 13. Fabricated sample of the proposed antenna: (a) top view and (b) 3D view.

a 3.5-mm coaxial calibration standard GCS35M were used to measure the antenna's reflection coefficient. Far-field measurements were carried out at the RFID/USN Center, Incheon, Korea. A full anechoic chamber with a size of 15.2 m (W) × 7.9 m (L) × 7.9 m (H) and an Agilent E8362B network analyzer were used in pattern measurement. The proposed antenna was used for reception and a standard wideband horn antenna for transmission. A transmission distance of 10 m was established between both antennas. With a scan angle of 1° and a speed of 3°/s, the designed antenna was rotated from −180° to 180° while keeping the horn antenna fixed.

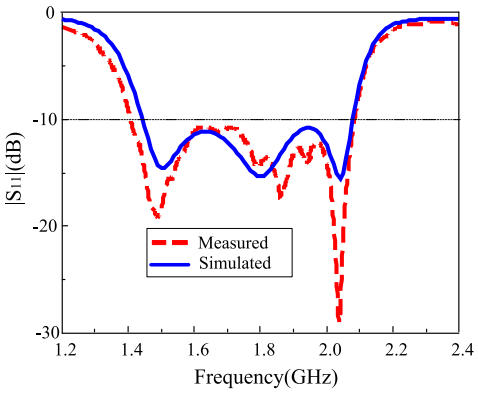

FIGURE 14. Measured and simulated $|S_{11}|$ values.

Fig. 14 shows the measured and simulated reflection coefficients for the fabricated antenna. There exist minute

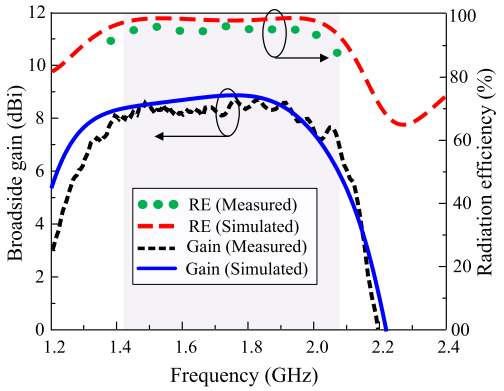

FIGURE 15. Simulated and measured broadside gain with radiation efficiency of the dipole antenna loaded with parasitic patches and folded strips.

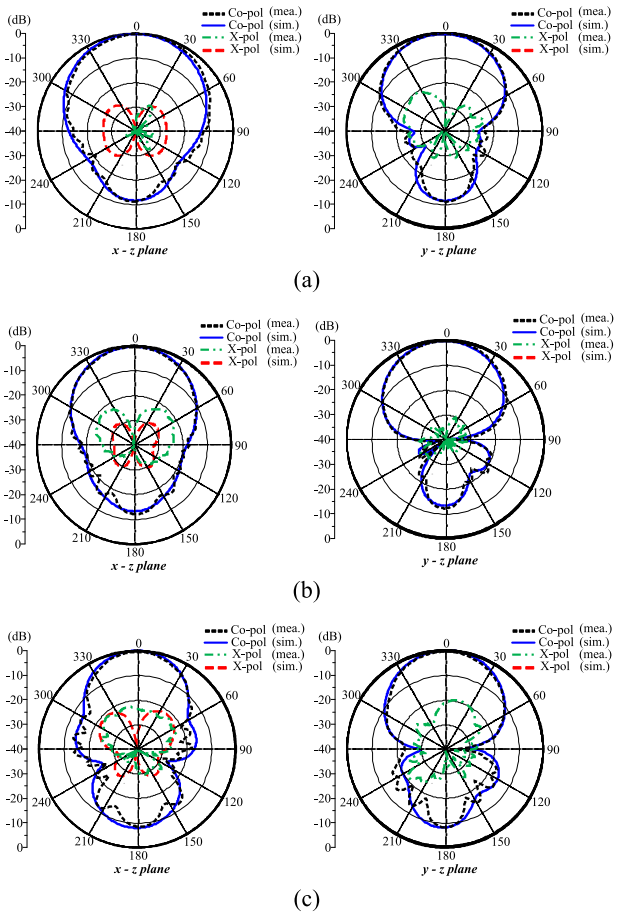

FIGURE 16. Simulated and measured normalized radiation patterns of the single dipole antenna loaded with parasitic patches and folded strips: (a) 1.5 GHz, (b) 1.8 GHz, and (c) 2.02 GHz.

disparities between the measurements and the HFSS simulation, which could be a consequence of a slight alignment error during the fabrication. As shown in Fig. 14, the measured impedance bandwidth for $|S_{11}| < -10$ dB is 1.39–2.09 GHz (40.22%), and the simulated bandwidth is 1.44–2.08 GHz (36.36%).

TABLE 1. Performance comparison of the proposed antenna with other antenna designs.

Antenna structure	Size(λ^3)	BW (%)	Peak gain (dBi)	RE (%)
Ref. [2][1]	0.5 × 0.5 × 0.05	0.07	5.2	-
Ref. [13][1]	0.65 × 0.78 × 0.06	8.2	7.1	90
Ref. [15][1]	0.9 × 0.9 × 0.07	16	6.7	-
Ref. [20][5]	1.8 × 1.8 × 0.02	2.2	8.7	97
Ref. [21][1]	1.5 × 1.5 × 0.05	0.6	7.8	74
Ref. [22][1]	0.64 × 0.64 × 0.087	17.2	8.8	96
Ref. [31][4]	1.643 × 1.643 × 0.230	85	8	-
Ref. [32][2]	1.21 × 0.93 × 0.36	88	10.06	-
Ref. [33][3]	0.703 × 0.367 × 0.253	40	7.6	90
Ref. [35][4]	1.0 × 1.0 × 0.097	28.6	10.3	-
Ref. [36][1]	1.198 × 1.198 × 0.253	10	8.5	83
Proposed[1]	0.69 × 0.69 × 0.094	40.22	8.2	88

[1]$S_{11}\leq -10$ dB, [2]$S_{11}\leq -15$ dB, [3]VSWR≤1.5, [4]VSWR≤2, [5]VSWR≤3

The broadside gain and radiation patterns of the fabricated prototype at different frequencies were measured and are shown in Figs. 15 and 16. Fig. 15 shows the comparison between the simulated and measured broadside gain and radiation efficiency of the fabricated antenna. The measurements resulted in a peak gain of 8.2 dBi and high radiation efficiency of >88% across the operational bandwidth.

The radiation patterns with a high front-to-back ratio were quite symmetric in both the *x*–*z* and *y*–*z* planes. At 1.5 GHz, the measurements resulted in a broadside gain of 7.71 dBi; HPBWs of 79.9° and 66.07° in the *x*-*z* and *y*-*z* planes, respectively; and a front-to-back ratio of 11.23 dB. At 1.8 GHz, the prototype yielded a measured broadside gain of 8.22 dBi; HPBWs of 58.63° and 60.93° in the *x*-*z* and *y*-*z* planes, respectively; and a front-to-back ratio of 12.3 dB. At 2.02 GHz, the measurements indicated a broadside gain of 6.92 dBi; HPBWs of 45.76° and 55.31° in the *x*–*z* and *y*-*z* planes, respectively; and a front-to-back ratio of 8.73 dB.

Table 1 compares the performance of the proposed antenna to that of the other low-profile antenna designs described in the literature.

V. CONCLUSION

A method for improving the impedance bandwidth of a low-profile planar radiating element placed horizontally in proximity above the ground plane is presented. The antenna comprises a dipole, folded strips, and four parasitic patches with a corner cut at each edge. The effects of the folded strips are significant in increasing the impedance bandwidth by producing additional resonance. The parasitic patches are functional in phase compensation while improving the bandwidth by resonating at low frequency. The corner cut on the parasitic patches enhances coupling and expands the usable bandwidth. With radiating elements very close to the ground plane with a spacing of $0.094\lambda_o$, the antenna yields excellent performance. The increase in bandwidth resulting from the folded strips and parasitic patches was computationally and experimentally verified, which validates the antenna design. The proposed antenna design is simple and easy to implement, especially when considering the notable bandwidth improvement, particularly at a low profile.

REFERENCES

[1] S. S. S. Nasser, W. Liu, and Z. N. Chen, "Wide bandwidth and enhanced gain of a low-profile dipole antenna achieved by integrated suspended metasurface," *IEEE Trans. Antennas Propag.*, vol. 66, no. 3, pp. 1540–1544, Mar. 2018.

[2] Y. Huang, A. De, Y. Zhang, T. K. Sarkar, and J. Carlo, "Enhancement of radiation along the ground plane from a horizontal dipole located close to it," *IEEE Antennas Wireless Propag. Lett.*, vol. 7, pp. 294–297, 2008.

[3] S. R. Best and D. L. Hanna, "Design of a broadband dipole in close proximity to an EBG ground plane," *IEEE Antennas Propag. Mag.*, vol. 50, no. 6, pp. 52–64, Dec. 2008.

[4] F. Yang and Y. Rahmat-Samii, *Electromagnetic Band Gap Structures in Antenna Engineering*. London, U.K.: Cambridge Univ. Press, 2008.

[5] I. Park, "Application of metasurfaces in the design of performance-enhanced low-profile antennas," *EPJ Appl. Metamaterials*, vol. 5, no. 11, pp. 1–13, Nov. 2018.

[6] M. Li, Q. L. Li, B. Wang, C. F. Zhou, and S. W. Cheung, "A low-profile dual-polarized dipole antenna using wideband AMC reflector," *IEEE Trans. Antennas Propag.*, vol. 66, no. 5, pp. 2610–2615, May 2018.

[7] H. H. Tran and I. Park, "A dual-wideband circularly polarized antenna using an artificial magnetic conductor," *IEEE Antennas Wireless Propag. Lett.*, vol. 15, pp. 950–953, 2016.

[8] C. A. Balanis, *Antenna Theory: Analysis and Design*, 4th ed. New York, NY, USA: Wiley, 2016.

[9] F. Yang and Y. Rahmat-Samii, "Reflection phase characterizations of the EBG ground plane for low profile wire antenna applications," *IEEE Trans. Antennas Propag.*, vol. 51, no. 10, pp. 2691–2703, Oct. 2003.

[10] H. Mosallaei and K. Sarabandi, "Antenna miniaturization and bandwidth enhancement using a reactive impedance substrate," *IEEE Trans. Antennas Propag.*, vol. 52, no. 9, pp. 2403–2414, Sep. 2004.

[11] M. Z. Azad and M. Ali, "Novel wideband directional dipole antenna on a mushroom like EBG structure," *IEEE Trans. Antennas Propag.*, vol. 56, no. 5, pp. 1242–1250, May 2008.

[12] S. Nelaturi and N. Sarma, "A compact microstrip patch antenna based on metamaterials for Wi-Fi and WiMAX applications," *J. Electromagn. Eng. Sci.*, vol. 18, no. 3, pp. 182–187, Jul. 2018.

[13] A. Vallecchi, J. R. De Luis, F. Capolino, and F. De Flaviis, "Low profile fully planar folded dipole antenna on a high impedance surface," *IEEE Trans. Antennas Propag.*, vol. 60, no. 1, pp. 51–62, Jan. 2012.

[14] M. F. Abedin and M. Ali, "Effects of EBG reflection phase profiles on the input impedance and bandwidth of ultrathin directional dipoles," *IEEE Trans. Antennas Propag.*, vol. 53, no. 11, pp. 3664–3672, Nov. 2005.
[15] I. T. McMichael, A. I. Zaghloul, and M. S. Mirotznik, "A method for determining optimal EBG reflection phase for low profile dipole antennas," *IEEE Trans. Antennas Propag.*, vol. 61, no. 5, pp. 2411–2417, May 2013.
[16] M. Li, S.-Q. Xiao, J. Xiong, and B.-Z. Wang, "Horizontal dipole located close to ground plane with bidirectional endfire radiation," *IEEE Antennas Wireless Propag. Lett.*, vol. 13, pp. 1144–1147, 2014.
[17] D. Sievenpiper, L. Zhang, R. F. J. Broas, N. G. Alexopolous, and E. Yablonovitch, "High-impedance electromagnetic surfaces with a forbidden frequency band," *IEEE Trans. Antennas Propag.*, vol. AP-47, no. 11, pp. 2059–2074, Nov. 1999.
[18] F. Costa, O. Luukkonen, C. R. Simovski, A. Monorchio, S. A. Tretyakov, and P. M. de Maagt, "TE surface wave resonances on high-impedance surface based antennas: Analysis and modeling," *IEEE Trans. Antennas Propag.*, vol. 59, no. 10, pp. 3588–3596, Oct. 2011.
[19] S. R. Best, "A novel element and feed configuration for a dipole very closely spaced to a PEC ground plane," in *Proc. Antennas Propag. Soc. Symp.*, vol. 3, Jun. 2004, pp. 2907–2910.
[20] S. R. Best, "Improving the performance properties of a dipole element closely spaced to a PEC ground plane," *IEEE Antennas Wireless Propag. Lett.*, vol. 3, no. 1, pp. 359–363, Dec. 2004.
[21] Z. Chen, Y. Juan, X. Qing, and W. Che, "Enhanced radiation from a horizontal dipole closely placed above a PEC ground plane using a parasitic strip," *IEEE Trans. Antennas Propag.*, vol. 64, no. 11, pp. 4868–4871, Nov. 2016.
[22] S. X. Ta, K. E. Kedze, D. N. Chien, and I. Park, "Bandwidth-enhanced low-profile antenna with parasitic patches," *Int. J. Antennas Propag.*, vol. 2017, Nov. 2017, Art. no. 6529060.
[23] M. G. N. Alsath and N. Kanagasabai, "Compact UWB monopole antenna for automotive communication," *IEEE Trans. Antennas Propag.*, vol. 63, no. 9, pp. 4204–4208, Sep. 2015.
[24] H.-W. Liu, C.-H. Ku, T.-S. Wang, and C.-F. Yang, "Compact monopole antenna with band-notched characteristic for UWB applications," *IEEE Antennas Wireless Propag. Lett.*, vol. 9, pp. 397–400, 2010.
[25] K. R. Chen, C. Y. D. Sim, and J. S. Row, "A compact monopole antenna for super wideband applications," *IEEE Antennas Wireless Propag. Lett.*, vol. 10, pp. 488–491, 2011.
[26] S. Nikolaou and M. A. B. Abbasi, "Design and development of a compact UWB monopole antenna with easily-controllable return loss," *IEEE Trans. Antennas Propag.*, vol. 65, no. 4, pp. 2063–2067, Apr. 2017.
[27] L. Ge and K. M. Luk, "A wideband magneto-electric dipole antenna," *IEEE Trans. Antennas Propag.*, vol. 60, no. 11, pp. 4987–4991, Nov. 2012.
[28] L. Ge and K. M. Luk, "A magneto-electric dipole antenna with low-profile and simple structure," *IEEE Antennas Wireless Propag. Lett.*, vol. 12, pp. 140–142, 2013.
[29] L. Ge and K.-M. Luk, "A low-profile magneto-electric dipole antenna," *IEEE Trans. Antennas Propag.*, vol. 60, no. 4, pp. 1684–1689, Apr. 2012.
[30] J. Zeng and K.-M. Luk, "A simple wideband magnetoelectric dipole antenna with a defected ground structure," *IEEE Antennas Wireless Propag. Lett.*, vol. 17, no. 8, pp. 1497–1500, Aug. 2018.
[31] X. Cui, F. Yang, M. Gao, L. Zhou, Z. Liang, and F. Yan, "A wideband magnetoelectric dipole antenna with microstrip line aperture-coupled excitation," *IEEE Trans. Antennas Propag.*, vol. 65, no. 12, pp. 7350–7354, Dec. 2017.
[32] L. Chang, J.-Q. Zhang, L.-L. Chen, and B.-M. Li, "Bandwidth-enhanced cavity-backed magneto-electric dipole antenna," *IEEE Access*, vol. 6, pp. 62482–62489, 2018.
[33] L. Ge and K. M. Luk, "Beamwidth reconfigurable magneto-electric dipole antenna based on tunable strip grating reflector," *IEEE Access*, vol. 4, pp. 7039–7045, 2016.
[34] G. Idayachandran and R. Nakkeeran, "Compact magneto-electric dipole antenna for LTE femtocell base stations," *Electron. Lett.*, vol. 52, no. 8, pp. 574–576, Apr. 2016.
[35] C. Ding and K. M. Luk, "Low-profile magneto-electric dipole antenna," *IEEE Antennas Wireless Propag. Lett.*, vol. 15, pp. 1642–1644, 2016.
[36] L. Ge and K.-M. Luk, "Linearly polarized and dual-polarized magneto-electric dipole antennas with reconfigurable beamwidth in the H-plane," *IEEE Trans. Antennas Propag.*, vol. 64, no. 2, pp. 423–431, Feb. 2016.
[37] K. E. Kedze, H. Wang, and I. Park, "Broadband low-profile dipole antenna with parasitic patches and folded strips," in *Proc. APS-URSI Int. Symp. Antennas Propag.*, Boston, MA, USA, Jul. 2018, pp. 1733–1734.
[38] S. X. Ta, I. Park, and R. W. Ziolkowski, "Broadband electrically small circularly polarized directive antenna," *IEEE Access*, vol. 5, pp. 14657–14663, 2017.

KAM EUCHARIST KEDZE received the B.Tech. degree in electrical and electronic engineering (tele-communication) degree from the University of Buea, Cameroon, in 2013. He is currently pursuing the joint M.S./Ph.D. degree with the Department of Electrical and Computer Engineering, Ajou University, Suwon, South Korea. His research interests include the design of patch antennas, crossed-dipole antennas, miniaturized antennas, and metasurface antennas.

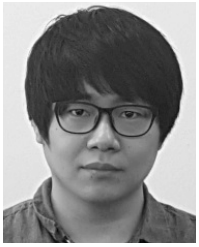

HEESU WANG received the B.Sc. degree in electrical and computer engineering from Ajou University, Suwon, South Korea, in 2018, where he is currently pursuing the M.S. degree with the Department of Electrical and Computer Engineering. His research interests include the design of patch antennas, printed antennas, small antennas, and metasurface antennas for various wireless applications.

SON XUAT TA received the B.Sc. (Eng.) degree in electronics and telecommunications from the Hanoi University of Science and Technology, Hanoi, Vietnam, in 2008, and the Ph.D. degree in electrical engineering from Ajou University, Suwon, South Korea, in 2016, where he was a Postdoctoral Research Fellow with the Department of Electrical and Computer Engineering, from 2016 to 2017. He is currently with the School of Electronics and Communications, Hanoi University of Science and Technology. He has authored or co-authored over 70 technical journal and conference papers. His recent research interests include antennas, metamaterials, metasurfaces, metamaterial-based antennas, metasurface-inspired antennas, circularly polarized antennas, and millimeter-wave antennas and arrays.

IKMO PARK received the B.S. degree in electrical engineering from The State University of New York at Stony Brook and the M.S. and Ph.D. degrees in electrical engineering from the University of Illinois at Urbana–Champaign. He was with the Device and Materials Laboratory, LG Corporate Institute of Technology, Seoul, South Korea, where he was engaged in the research and development of various antennas for personal communication systems, wireless local area networks, and direct broadcasting systems. He joined the Department of Electrical and Computer Engineering, Ajou University, Suwon, South Korea, in 1996. He was a Visiting Professor with the Department of Electrical and Computer Engineering, POSTECH, Pohang, South Korea, from 2004 to 2005, and with the Department of Electrical and Computer Engineering, The University of Arizona, Tucson, AZ, USA, from 2011 to 2012.

He was the Chair of the Department of Electrical and Computer Engineering, Ajou University. He has authored or co-authored over 300 technical journal and conference papers. He holds over 40 domestic and international patents. His current research interests include the design and analysis of microwave, millimeter-wave, terahertz wave, and nano-structured antennas with metamaterials and metasurfaces. He is also a member of Eta Kappa Nu and Tau Beta Pi. He serves as the Program Manager for the Information and Communications Technology Sector at the National Research Foundation of Korea. He also serves as the Chair, an Organizer, and a member of program committees for various conferences, workshops, and short courses in electromagnetic-related topics. He is one of the Board of Directors at the Korea Institute of Electromagnetic Engineering and Science (KIEES). He serves as the Editor-in-Chief for the *Journal of KIEES*, an Editorial Board Member of the *International Journal of Antennas and Propagation*, and an Associate Editor for *IET Electronics Letters*. He has served as the Editor-in-Chief for the *Proceeding of the KIEES* and an Editorial Board Member of the *Journal of Electromagnetic Engineering and Science*. He is also a frequent Reviewer for many scientific journals and book publishers.

Dr. Park was a recipient of several awards and recognitions, including the Haedong Best Paper Award from the Institute of Electronics Engineers of Korea, in 2002, the IEEE iWAT Best Poster Paper Award in 2005, the Outstanding Advisor Award from the Radio Engineering and Research Center, KAIST, in 2009, the Best Paper Award from the Optical Society of Korea, in 2007, the Best Paper Award from KIEES, in 2010 and 2016, the Distinguished Service Award from the Department of Electrical and Computer Engineering, Ajou University, in 2011, the KIEES Outstanding Researcher Award, in 2013, the Ajou Publication Award, in 2013, the KIEES Scholarly Achievement Award, in 2014, the KIEES Distinguished Service Award, in 2012 and 2018, the KIEES Meritorious Award, in 2015, and the Ajou Dasan Research Award, in 2017 and 2018.